




# The Effect of Ion Exchange Poisoning on the Ion Transport and Conduction in Polymer Electrolyte Membranes (PEMs) for Water Electrolysis

Maximilian Schalenbach,<sup>1,z</sup>  Lilli Keller,<sup>1,2</sup> Benjamin Janotta,<sup>1,3</sup> Alexander Bauer,<sup>1</sup> Hermann Tempel,<sup>1</sup> Hans Kungl,<sup>1</sup> Martin Bonnet,<sup>2</sup> and Rüdiger-A. Eichel<sup>1,3</sup>

<sup>1</sup>Fundamental electrochemistry (IEK-9), Institute of Energy and Climate Research, Forschungszentrum Jülich, Wilhelm-Johnen-Straße, 52425 Jülich, Germany

<sup>2</sup>TH Köln, Betzdorfer Str. 2, 50679 Cologne, Germany

<sup>3</sup>RWTH Aachen University, Institute of Physical Chemistry, 52062 Aachen, Germany

In water electrolyzers, polymer electrolyte membranes (PEMs) such as Nafion can accumulate cations stemming from salt impurities in the water supply, which leads to severe cell voltage increases. This combined experimental and computational study discusses the influence of sodium ion poisoning on the ionic conductivity of Nafion membranes and the ion transport in a thereon based water electrolysis cell. Conductivities of Nafion and aqueous solutions with the same amount of dissolved cations are measured with impedance spectroscopy and compared with respect to Nafion's microstructure. The dynamic behavior of the voltage of a water electrolysis cell is characterized as a function of the sodium ion content and current density, showing the differences of the ion transport at alternating and direct currents. These experimental results are elucidated with a physical ion transport model for sodium ion poisoned Nafion membranes, which describes a proton depletion and sodium ion accumulation at the cathode. During proton depletion, the cathodic hydrogen evolution is maintained by the water reduction that forms hydroxide ions. Together with sodium ions from the membrane, the formed hydroxide ions can diffuse pairwise into the water supply, so that the membrane's sodium ions can be at least partly be replaced with anodically formed protons.

© 2022 The Author(s). Published on behalf of The Electrochemical Society by IOP Publishing Limited. This is an open access article distributed under the terms of the Creative Commons Attribution 4.0 License (CC BY, <http://creativecommons.org/licenses/by/4.0/>), which permits unrestricted reuse of the work in any medium, provided the original work is properly cited. [DOI: 10.1149/1945-7111/ac9087]



Manuscript submitted May 6, 2022; revised manuscript received June 27, 2022. Published September 20, 2022.

Supplementary material for this article is available [online](#)

Low temperature water electrolysis employing polymer electrolyte membranes (PEMs) or alkaline electrolytes is considered as a key technology for a renewable economy.<sup>1–3</sup> Proton exchange PEMs typically have sulfonic acid groups<sup>4,5</sup> that are covalently bonded to a polymer matrix. The polar nature of the functional groups allows water uptake in PEMs, which leads to a nanoscale separation between the polymeric phase and the water channels.<sup>6,7</sup> The dissociated protons in the aqueous phase are mobile and thus provide ionic conductivity to which the immobile anions do not contribute.<sup>8,9</sup> The state-of-the-art proton exchange membrane for water electrolysis is Nafion,<sup>6,10,11</sup> a perfluorinated sulfonic acid, which is chemically stable and mechanically robust.<sup>12,13</sup> The intrinsic ionic conductivity of PEMs allows the operation of water electrolyzers with a deionized water supply without conductive electrolytic additives.<sup>14</sup>

The electrodes in PEM water electrolyzers typically consist of a mixture of a polymeric electrolyte phase and catalyst nanoparticles,<sup>15–17</sup> while catalyst support materials, such as carbon for the cathode, can improve the electronic conductivity in these layers. Thin membranes with thicknesses that range between 25 and 250  $\mu\text{m}$  are typically used for PEM water electrolyzers,<sup>12,18</sup> so that the cells exhibit low resistances. However, a major issue of PEM water electrolysis is that the membrane can be contaminated or poisoned by salts from the water supply.<sup>12,19,20</sup> Traces of, e.g., sodium chloride can lead to sodium ion accumulation in the membrane.<sup>21,22</sup> Zhang et al.<sup>20,23</sup> examined the effect of sodium chloride in the supply water and its effect on the cell voltage. Babic et al.<sup>24</sup> reported that  $\text{CO}_2$  can be used to regenerate PEMs with metal ion impurities in water electrolyzers.

The ion movement that is driven by the electric field and diffusion leads to concentration gradients in liquid electrolytes<sup>25–27</sup> which can be precisely modeled.<sup>28</sup> Nafion in the fully hydrated state (immersed in water) is reported to have a proton concentration of 2.7 M in the aqueous phase and a six-fold lower conductivity as that of acids with the same proton concentrations.<sup>29</sup> The main share of

the difference in the conductivities was attributed to geometric restrictions of the ion transport in Nafion's water channels.<sup>29</sup> Despite the geometric restrictions for the ion transport in the water channels, the models for the ions in aqueous solutions might be adaptable to describe the ion transport in Nafion. In particular, the case of a poisoned membrane displays a multi-ion system which was recently modeled for liquid electrolytes.<sup>30</sup> Zlobinski et al.<sup>31</sup> examined the cation impurities in PEM water electrolyzers for a  $\text{Gd}^{3+}$  ion with dynamic neutron imaging, showing a cathodic accumulation of the cation impurities that was also described by a simple numerical model.

The aim of this study is to understand how ion exchange poisoning impacts the ion transport in PEMs under alternating and direct currents, exemplified for Nafion based PEM water electrolysis. Within this scope, the ionic conductivity is measured as a function of the sodium ion content with impedance spectroscopy, which probes the current response of the equilibrated membrane at alternating voltage perturbations. The ion rearrangement in the membrane under direct currents is computationally modeled, for which previously reported models are adapted and applied to a Nafion membrane with sodium ion poisoning, including the proton and sodium ion movements in the PEM and their interaction with the local electroneutrality with respect to the non-mobile covalently bonded anions of the sulfonic groups. The computational results are related to time-dependent voltage profiles of PEM water electrolysis cells and the electrode reactions. The voltage characteristics of the electrolysis cell are thoroughly examined as a function of the sodium ion content and the current density, showing how the ion transport in the membrane affects the electrocatalytic reactions and how the altered electrode reactions partly lead to a sodium ion transfer from the membrane into the water supply. The observed cell characteristics can be used to estimate the state of the sodium ion poisoning of water electrolysis cells with Nafion membranes. The sodium ion accumulation in the PEM over time is discussed as a function of the sodium chloride content of the supply water and the employed current density, showing at which time scales this phenomenon is expected to affect the performance of water electrolysis cells during application.

<sup>z</sup>E-mail: [m.schalenbach@fz-juelich.de](mailto:m.schalenbach@fz-juelich.de)

## Methods

**Ionic conductivity at alternating currents.**—Membrane specimens of 1.5 cm width and 12 cm length were cut from Nafion NR212 and N115 sheets (purchased from Alfa Aesar). A previously reported four-point impedance measurement technique was employed to measure the ionic conductivity of Nafion membrane specimens immersed in ultrapure water.<sup>29,32</sup> A schematic sketch of the measurement cell is presented in the supporting information. From the impedance spectra, the resistance  $R$  was determined with the procedure described in the literature in detail.<sup>29,32</sup> The conductivities of the membrane specimens  $\kappa$  were then calculated by taking into account the specimen's geometry that is measured in the fully hydrated state:

$$\kappa = \frac{l}{RA} \quad [1]$$

The ionic conductivity measurement of each membrane specimen was repeated five times at a temperature of 20 °C. Three membrane specimens with an identical sample preparation procedure were examined for every sodium ion content considered. One of these series consisted of NR212 specimen, the two other of N115 specimen. Each of these specimen was measured for three times. The measurement error was determined by the standard variance of the measured ionic conductivities.

The conductivities of aqueous solutions with a similar ion composition as the electrolyte in the aqueous phase of sodium-ion poisoned Nafion membranes was measured with a Mettler Toledo conductometer (Seven Compact Series). To calculate the contributions of the cations to the conduction of these aqueous solutions, first the transference numbers for the sodium ions  $t_{\text{Na}^+}$  and protons  $t_{\text{H}^+}$  were calculated on the basis of the molar conductivities  $\Lambda$  and concentrations  $c$  of the ion types that are reported in the literature.<sup>33</sup>

$$t_{\text{Na}^+} = \frac{\Lambda_{\text{Na}^+} c_{\text{Na}^+}}{\Lambda_{\text{Na}^+} c_{\text{Na}^+} + \Lambda_{\text{H}^+} c_{\text{H}^+} + \Lambda_{\text{Cl}^-} c_{\text{Cl}^-}} \quad [1a]$$

$$t_{\text{H}^+} = \frac{\Lambda_{\text{H}^+} c_{\text{H}^+}}{\Lambda_{\text{Na}^+} c_{\text{Na}^+} + \Lambda_{\text{H}^+} c_{\text{H}^+} + \Lambda_{\text{Cl}^-} c_{\text{Cl}^-}} \quad [2]$$

The total conductivity of the cations  $\kappa_{\text{cations}}$  as a function of the measured conductivity  $\kappa$  was then calculated by:

$$\kappa_{\text{cations}} = (t_{\text{Na}^+} + t_{\text{H}^+})\kappa \quad [3]$$

A drawback of this approach are the high errors, as the transference numbers and single molar conductances are reported for infinite solutions and expected to change towards the high molar electrolytes that are measured in this study. Moreover, the ion-ion interactions in multi-ion system are complex<sup>30</sup> and their theoretical understanding is limited.<sup>34</sup> As a result, the outcome of Eq. 3 can be interpreted as a rough estimation.

**Water uptake.**—To determine the water uptake  $\lambda$ , the membrane specimens were weighed in the dry state at controlled ambient temperature of 20 °C and humidity below 40%. Previously, the membrane samples were immersed in ultrapure water for at least an hour. The weight of the fully hydrated membrane specimen was measured directly after removing the specimen from the water immersion. The water uptake was then correlated with the amount of available functional groups based on the equivalent weight of the dry specimen. By this procedure, the wetted surface of the specimen and the fast water evaporation at the Nafion-air interface displays a measurement error.

**Electrolysis measurements.**—The electrochemical behavior of the ion transport through a membrane electrode assembly (MEA) under direct currents was examined with an in-house made

electrolysis cell (see supporting information for details). The MEA (purchased from Ion Power) had an active area of 17.6 cm<sup>2</sup>, consisting of a Nafion N117 membrane, Pt/C as the cathode catalyst, and iridium oxide as the anode catalyst. Two TPG-H-60 Toray papers were used as the cathode current collector, titanium meshes (Alfa Aesar) that were platinized in-house with a sputter coater were used as the anode current collector.

Three different measurement procedures were conducted with this cell: (i) The MEA was prepared with a 10% sodium ion content (as described below) and was afterwards thoroughly rinsed with ultrapure water and rested overnight. The next day a constant current density of 1 A cm<sup>-2</sup> was applied while the conductivity of the cathodic supply water was simultaneously measured. Separate ultrapure water supplies were employed for the anode and cathode, each with a volume of 150 ml. The flow rate in either electrode compartment was 100 ml min<sup>-1</sup>, pumped with peristaltic pumps in loops. A conductivity sensor (Mettler Toledo, InLab 742) was placed in the cathodic water supply vessel, in which the solution was stirred with a PTFE magnetic stirrer bar, to ensure that the conductivity sensor is in contact with an evenly mixed solution. The conductivity sensor was connected to a potentiostat (Biologic SP-300), which probed the sensor's impedance in the electrolyte solution at a frequency of 300 Hz (where the low conductivity solutions have a nearly pure Ohmic impedance with this sensor), enabling fast data tracking. The measured impedance of the sensor was correlated with the conductivity of the solution, using a calibrated conductometer (Mettler Toledo, Seven Compact Series) as a reference. The sodium ion removal from the membrane into the water supply was in addition examined with inductively coupled plasma optical emission spectroscopy (ICP-OES). (ii) After the previous measurement, the cell was rinsed with ultrapure water. Subsequently, again a current density of 1 A cm<sup>-2</sup> was applied, while the cell was operated with a run through supply of fresh ultrapure water. After the water supply passed the cell with a rate of 40 ml min<sup>-1</sup> in each compartment, the water was collected in plastic bottles for further ICP-OES analysis. (iii) The current density profile presented in Fig. 1 was applied to the cell to probe the ion transport in the electrolysis cell as a function of the sodium ion content. Between the current steps the cell was kept in an inactive state for 10 min without applying a current, so that concentration gradients inside the membrane were mostly equilibrated by diffusion. Each measurement thus started with negligible concentration gradients in the MEA, to ensure reproducible initial states. This procedure was applied for membranes with a sodium ion content of 0, 5, 10, 15 and 100%. After preparing each of these different sodium ion contents, the cell was rinsed with fresh ultrapure water and the water in the anodic and cathodic gas separators were exchanged. The volume of the recirculated anodic

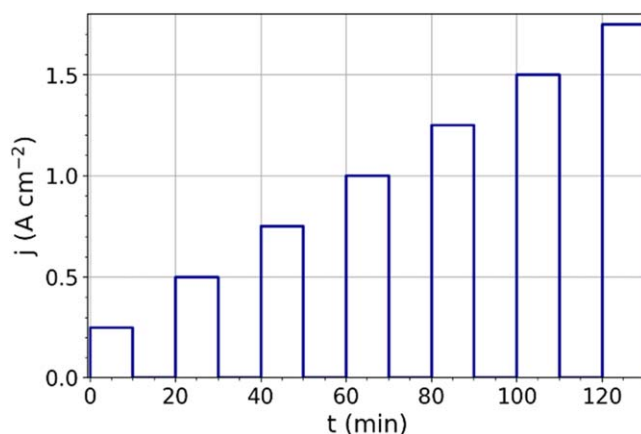


**Figure 1.** The current density profile that is applied to the electrolysis cell, to characterize the ion transport of the membrane electrode assemblies as a function of the sodium ion content.

and cathodic water supply were 200 ml each, pumped with a flow rate  $40 \text{ ml min}^{-1}$  through the cell, respectively.

**Cell resistance.**—The high frequency resistance of the cell of the electrolysis cell was measured via impedance spectroscopy, probed by an amplitude of 50 mV and a voltage of 1 V between the electrodes. By multiplying the measured high frequency resistance with the cell area, the area resistance of the cell was determined. First, the resistance of the cell without membrane was measured, leading to an area resistance of  $0.16 \Omega \text{ cm}^2$ . Afterwards, the area resistance of the cell with a MEA and various sodium ion contents was measured.

**Ion exchange procedure.**—The sodium ion content of the Nafion membranes was adjusted by two techniques: (i) By adding sodium chloride to the water supply of an electrolysis cell under direct currents as previously reported by Zhang et al.<sup>20,23</sup> In this case, the chlorine evolution at the anode leads to the permeation of sodium ions into the membrane. (ii) By the reaction of the acidic Nafion with a solution of a precisely adjusted amount of sodium hydroxide. This ion exchange procedure is preferred in this study, as it allows to adjust the sodium ion content of the membrane. Moreover, unlike the first approach, it can be performed without applying a current, which is later shown to influence the sodium ion content itself. A comparison of the results of both ion exchange approaches can be found in the supporting information.

The amount of sodium in the membrane was related to the total amount of cations in the membrane by the sodium ion fraction  $\xi_{\text{Na}^+}$ :

$$\xi_{\text{Na}^+} = \frac{c(\text{Na}^+)}{c(\text{Na}^+) + c(\text{H}^+)} \quad [5]$$

As specified by the manufacturer, the Nafion membranes have an equivalent weight of  $EW = 1100 \text{ g mol}^{-1}$ . The volume of sodium hydroxide  $V_{\text{NaOH}}$  required to achieve a certain mole fraction of sodium ions was calculated in relation to its concentration  $c_{\text{NaOH}}$  as a function of the mass of the Nafion specimen  $m_{\text{Nafion}}$  by:

$$V_{\text{NaOH}} = \xi_{\text{Na}^+} \frac{m_{\text{Nafion}}}{EW \times c_{\text{NaOH}}} \quad [6]$$

In the case of  $\xi_{\text{Na}^+} = 1$  (the  $\text{Na}^+$  form), 200% of the amount of sodium hydroxide necessary to replace all protons was used to replace the protons, to ensure that the membrane was completely transferred to the  $\text{Na}^+$  saturated state. After exposing the specimen to the sodium hydroxide solution, the specimens were rinsed with ultrapure water (resistance  $> 10^6 \Omega \text{ cm}$ ). The precision of the thus adjusted sodium ion content was estimated to approximately 15%, with respect to the measurement errors and the uncertainties of the precision of the equivalent weight. The concentration of ions  $c_{\text{ion}}$  in the aqueous phase is estimated with the concentration of water  $c_{\text{H}_2\text{O}} = 55.5 \text{ mol l}^{-1}$  by

$$c_{\text{ion}} \approx \frac{c_{\text{H}_2\text{O}}}{\lambda}, \quad [7]$$

with respect to a negligible influence of the dissolved ions on the density at the ion concentrations that are examined in this study.

The ion exchange of the Nafion membrane strips that are employed for the conductivity measurements is conducted by immersing the membrane samples in a covered plastic beaker filled with a sodium hydroxide solution (as described by Eq. 6) overnight. To adjust the sodium content of the MEA for the electrolysis measurements, the solution of sodium hydroxide (as described by Eq. 6) was pumped through the anodic flow field (the anodic titanium mesh is more permeable than the cathodic carbon paper) for four hours. The mass of the membrane was calculated with reference to the area weight of the membrane that is specified in the data sheet provided by the manufacturer. The mean of the active area

( $17.6 \text{ cm}^2$ ) and the total area ( $28 \text{ cm}^2$ , including the non-active MEA area beneath the sealing) served as a measure for the weight, as it is unclear how much of the sodium ions can penetrate into the non-active area of the MEA. The MEA was prepared with sodium hydroxide contents  $\xi_{\text{Na}^+}$  of 0.05, 0.1, 0.15 and 1, respectively. After the ion exchange, the cell was thoroughly purged with water to remove any excess sodium hydroxide. Before changing the sodium ion content, the MEA was transferred back to the  $\text{H}^+$  form by rinsing the cathodic and anodic water supply with 1 M sulfuric acid, followed by thorough rinsing with water.

**Ion transport model.**—A one-dimensional ion transport model for liquid electrolytes from the literature<sup>30</sup> is in the following adapted to describe the ion transport in the three-dimensional structure of the water channels in the Nafion membrane. The model for liquid electrolytes accounts for ion movement due to diffusion and electric field driven migration, considering the individual concentration-dependent ion mobility and local electroneutrality. In case of Nafion, the sulfonic anions are immobile, as they are covalently bonded to the polymer matrix.<sup>6</sup> The transport of cations in the water channels is calculated under the assumption that they behave analogously to their movement in aqueous solution, referring to previously reported<sup>29</sup> similarities of the conductivity in Nafion and aqueous solutions. The microstructure of the water channels is characterized by macroscopic properties in terms of the tortuosity and the volumetric water fraction in the literature.<sup>7,35,36</sup> By multiplying the tortuosity with the distance between the electrodes, the deviation of the ion transport pathways from a direct pathway due to the orientation of the water channels is included. By dividing the current density by the volumetric water fraction, the current density in the aqueous phase is decoupled from the non-conducting polymeric phase. Hence, the current density for the ion conduction in the aqueous phase is normalized to the geometric restrictions of the water channels. The model consists of 100 spatial compartments between the anode and cathode, while differential equations model the electric field and diffusion driven ion exchange between the compartments. In each of the compartments the total amount of anions and cations is equal to fulfil the local electroneutrality requirement, as in electrolytic conductors any deviation from electroneutrality is instantaneously balanced by the mobile ions.

In the following, the differential equations to model the ion transport are briefly discussed, for which the superscript index  $i$  describes an ion type and  $x$  denotes the spatial dimension in which the ions are conducted. A more detailed description can be found in previous works.<sup>28,30</sup> The molar flux  $\Phi^i$  of an ion type equals the sum of the contributions of diffusion  $\Phi_{\text{diff}}^i$  and electric field driven  $\Phi_{\text{el}}^i$  movement of the ions. Based on the continuity equation in the form of  $\frac{\partial c^i(x,t)}{\partial t} = -\frac{\partial \Phi^i(x,t)}{\partial x}$  the change of the spatiotemporal concentration can be related to the molar flux that is driven by the electric field and diffusion. The derivative of the molar flux in the spatial dimension equals:

$$\frac{\partial \Phi^i(x,t)}{\partial x} = \frac{\partial \Phi_{\text{diff}}^i(x,t)}{\partial x} + \frac{\partial \Phi_{\text{el}}^i(x,t)}{\partial x} \quad [8]$$

The derivative of the molar flux of the diffusion term that is described by Fick's first law equals:

$$\frac{\partial \Phi_{\text{diff}}^i(x,t)}{\partial x} = -D \frac{\partial^2 c^i(x,t)}{\partial x^2} \quad [9]$$

On the basis of Faraday law, the molar flux attributable to the Ohmic conduction equals the current density divided by the Faraday constant  $F$ :

$$\frac{\partial \Phi_{\text{el}}^i(x)}{\partial x} = \frac{1}{F z^i} \frac{\partial j^i}{\partial x} \quad [10]$$

The electroneutrality requires in every spatial element (subscript  $n$ ) of the simulation a negligible sum of the charges of the different ion types, which are described as the product of valency  $z$  and concentration  $c$ :

$$\sum_i z_n^i c_n^i(x, t) = 0 \quad [11]$$

A violation of the electroneutrality would lead to a strong electric field gradient that is instantaneously compensated by the conduction of the mobile ions. In the simulation, the movement of the ion is calculated with Eq. 8. Due to the different mobilities of the ions, small violations of the electroneutrality result after each iteration, which are numerically compensated by the contributions of the ions to the conductivity. A special boundary conditions for the electroneutrality is used for the ions in the spatial element at the cathode, which displays without the formation of hydroxides an impermeable barrier for sodium ions, for which the electroneutrality is here balanced by protons.

The sodium ion content affects the water uptake and thus sodium ion gradients in the membrane are expected to also lead to gradients of the water uptake. However, to describe these three-dimensional microstructure changes, an advanced modeling approach with respect to the structural transformation as a function of the sodium ion content is required. In this study, the system is simplified by modelling the ion transport for an even water uptake and a constant microstructure. Moreover, the dependence of the conductivities and diffusion coefficients of the mobile ions as a function of the sodium ion content are neglected, while the diffusion coefficients of the cations in the water channels are estimated as discussed below. With respect to these simplifications, the model shall serve as a semi-quantitative description of the ion transport in the PEM to understand the ion transport.

The proton conductivity of an aqueous solution with a concentration of 2.7 M - which is similar to the proton concentration in the aqueous phase of fully hydrated Nafion<sup>29</sup> - was previously estimated to approximately 1 S cm<sup>-1</sup> at 80 °C.<sup>29</sup> This value corresponds to molar conductivity of 370 S cm<sup>2</sup> mol<sup>-1</sup>. The mobility and conductivity of protons is approximately seven times higher than that of sodium ions,<sup>33,37</sup> which is attributable to the Grothuss mechanism and the smaller ion size and lower mass.<sup>38,39</sup> The molar conductivity of the sodium ions in Nafion is thus estimated to 53 S cm<sup>2</sup> mol<sup>-1</sup>. The diffusion coefficients were estimated with respect to these conductivities as described in the supporting information in detail. The mutual diffusion coefficients of salt ions, such as for sodium chloride for example, were reported to be almost three orders of magnitude lower in Nafion<sup>40</sup> than in aqueous solutions.<sup>33</sup> A detailed physicochemical explanation for this drastic difference has not yet been reported, but it might be attributable to scattering processes of diffusing ions at the walls of the water channels. In contrast, the diffusion coefficient estimated from conductivity measurements is similar to that of aqueous solutions when the geometric restrictions of the water channels are accounted for.<sup>29,40</sup> The diffusion coefficients of H<sup>+</sup> are assumed to equal that of aqueous solutions, as the proton diffusion is dominated by the Grothuss mechanism that impacts the conductivity in the same fashion. As discussed above, the detailed mechanisms of the cation diffusion in Nafion are yet not well understood, however, it is expected that the diffusion coefficients for the sodium ions in the water channels are between the reported values for the mutual pairwise diffusion in Nafion<sup>40</sup> and the diffusion in aqueous solutions. A good fit of the ion transport model to the experimental data is achieved with a 10 times smaller sodium ion diffusion coefficient than that expected from mobility in conductivity measurements. In the supporting information, the procedure to calculate the diffusion coefficients on the basis of the conductivities is discussed. The thus derived set of diffusion coefficients is later shown to adequately describe the ion transport with reference to the experimental measurements, yet, it is unclear whether this set of

**Table I. Model parameterization for three different sodium ion contents  $\xi_{\text{Na}^+}$ , including the concentration of ions in the aqueous phase  $c_{\text{aq}}$ , the volume fraction of water  $V_{\text{aq}}$  and the tortuosity of the water channels  $\tau$ .**

$\xi_{\text{Na}^+}$ (%)	$c_{\text{aq}}$ (M)	$V_{\text{aq}}$ (%)	$\tau$
5	2.8	37	2.1
10	3	35	2.2
15	3.1	34	2.2

parameters reflects the true transport properties in the water channels or whether this match is a result of coincidences.

The three-dimensional microstructure of the fully hydrated state of Nafion is discussed in the literature<sup>7,35,36,41-44</sup> as characterized by a tortuosity of 2 and a water uptake of approximately 40%. In the case of a sodium content of 10% the overall water uptake of the membrane is reduced by about 12% from approximately 21 water molecules per sulfonic group to 18.5 with reference to the data presented later. This decrease of the water uptake causes the overall concentration of ions in the aqueous phase to increase from 2.75 M in the fully hydrated state to approximately 3 M. The reduced water uptake decreases the volumetric water fraction to 35%. Moreover, the lower water uptake is assumed to increase the tortuosity from 2 to 2.2. Analogously, the values of the geometric properties were estimated for the sodium ion contents of 5% and 15%, as summarized in Table I.

During electrolysis, protons are produced at the anode and consumed at the cathode. The measurements with the electrolysis cell (see below) and the execution of the model are both conducted by employing constant currents. When protons deplete at the cathode, the constant current can be maintained by the reduction of water as the cathodic reaction. The water reduction yields hydroxides, which can penetrate into the membrane. If hydroxides and protons occur in the same spatial compartment of the simulation, they eliminate each other. The total amount of sodium in the membrane is kept constant in the model. Therefore, the diffusion of sodium hydroxide towards the water supply is not considered in the model, as discussed below in detail. The source code of the model is provided in the supporting information. The model may be in the future also applicable to describe the ion movement in concentration gradients in several kinds of electrochemical process with PEM membranes such as CO<sub>2</sub> reduction<sup>45</sup> or alkaline PEM water electrolysis.<sup>37</sup>

## Results and Discussion

First, water uptake and conductivity of Nafion are examined as a function of the sodium ion content. Second, the resistances of an water electrolysis cell is compared to the four point probed resistances of the Nafion specimen. Third, modeled concentration gradients of protons and sodium ions in the membrane under direct currents are discussed. Fourth, the physicochemical processes that are described by the model are used to elucidate the experimental data on the voltage of a water electrolysis cell as a function of time. Fifth, current density and sodium ion content are varied in the water electrolysis cell. Sixth, the implications of the findings with respect to the application in industrial water electrolysis are discussed.

### Conductivity at alternating currents and water uptake.—

Figure 2A shows the water uptake of Nafion after immersion in water as a function of the sodium ion content  $\xi_{\text{Na}^+}$ . The water uptake  $\lambda$  in the H<sup>+</sup> state is approximately 21% and decreases to 14% in the Na<sup>+</sup> state. The results reproduce previously reported results on the effect of sodium ions on the water uptake.<sup>46,47</sup> The physicochemical reasons for the lower water uptake with increasing sodium ion content were discussed in the literature.<sup>47,48</sup>

The decreasing water content due to higher sodium ion contents implies an ion concentration increase in the aqueous phase with respect to Eq. 7.

Figure 2B shows that the conductivity decreases with a higher sodium ion uptake, in agreement with previously reported measurements.<sup>46,49,50</sup> The conductivity of the Nafion specimen is determined on the basis of electrochemical impedance spectroscopy, which probes the membrane specimens under perturbations of equilibrated states with an amplitude of 50 mV, which means that the electric field driven ion movements during the measurements do not form macroscopic concentration gradients. When the membrane specimen in the Na<sup>+</sup> form are immersed in sulfuric acid and thoroughly rinsed with ultrapure water, they show the same conductivity as in the initial H<sup>+</sup> form (see data in the supporting information). Thus, the ion exchange procedure is fully reversible. A non-linear correlation between the conductivity and the sodium ion content is observed, as pointed out by the guide for the eye in Fig. 2B, which is related to the physicochemical effects discussed in the following.

Figure 2C shows the conductivity of the Nafion membrane from Fig. 2B in comparison to that of aqueous solutions of hydrochloric acid and sodium chloride with the same proton and sodium concentration as that of the aqueous phase of the prepared Nafion specimens. In this context, the data from Fig. 2A in combination with Eq. 7 serve as a measure for the concentration of the ions in the aqueous phase of Nafion. As the water uptake decreases with higher sodium ion contents, the overall ion concentration increases in the aqueous phase of Nafion. To resolve the differences of the conductivity of Nafion and aqueous solutions as a function of the sodium ion content in more detail, Fig. 2D shows the ratio of the two conductivities. In aqueous solutions at infinite dilution, protons are seven times more mobile than sodium ions,<sup>33,37</sup> for which the contribution of chloride ions to the conductivity of the aqueous solutions increases towards larger fraction of sodium ion content. While the chloride anions in the aqueous solutions are mobile, the sulfonic acid groups of the Nafion membrane are immobile. Hence, to compare the cation transport in Nafion and aqueous solution in more detail, the conductance of the anions is deducted from the aqueous solutions with the procedure presented above. The thus obtained ratio is also graphed in Fig. 2D and shows a six to nine times higher conductivity of the cations in the aqueous solutions than that of Nafion. As the estimation of the chloride ion movement is affected by large errors, a detailed quantitative discussion of the differences of the cation ion conduction in the aqueous solution and Nafion is thus not possible.

The differences of the cation conductivities of Nafion and aqueous solutions as a function of the sodium ion mole fraction are associated here with the following physicochemical effects: (i) The available effective cross-section for the ion conduction decreases with lower water uptakes. (ii) The tortuosity of the water channels increases with a lower water uptake. Thus, the length of the ion conduction pathways through the three dimensional microstructure of Nafion increases, and the directions of said pathways become less uniform as a result of the lower water uptake due to higher sodium ion contents. (iii) Less water uptake increases the interaction between moving ions and the polymeric phase and functional groups. Thus, the proton transport is hindered. (iv) The sodium ions with their hydration shells may impede the movement of protons, thus influencing their mobility, which is in aqueous solutions at infinite dilution approximately seven times higher compared to that of the sodium ions.<sup>33,37</sup> In the concentrated and confined electrolyte in the water channels of Nafion, the differences change, however, the trend of a significantly more conducting proton remains. This difference may more drastically affect the ion movement in the aqueous phase in Nafion relative to aqueous solutions, as both ion types must share the same routes through the three dimensional nanostructure of Nafion whereas in aqueous solutions enough space for alternative pathways is accessible. (v) The contributions of the Grothuss<sup>38,39</sup> and vehicle mechanisms may

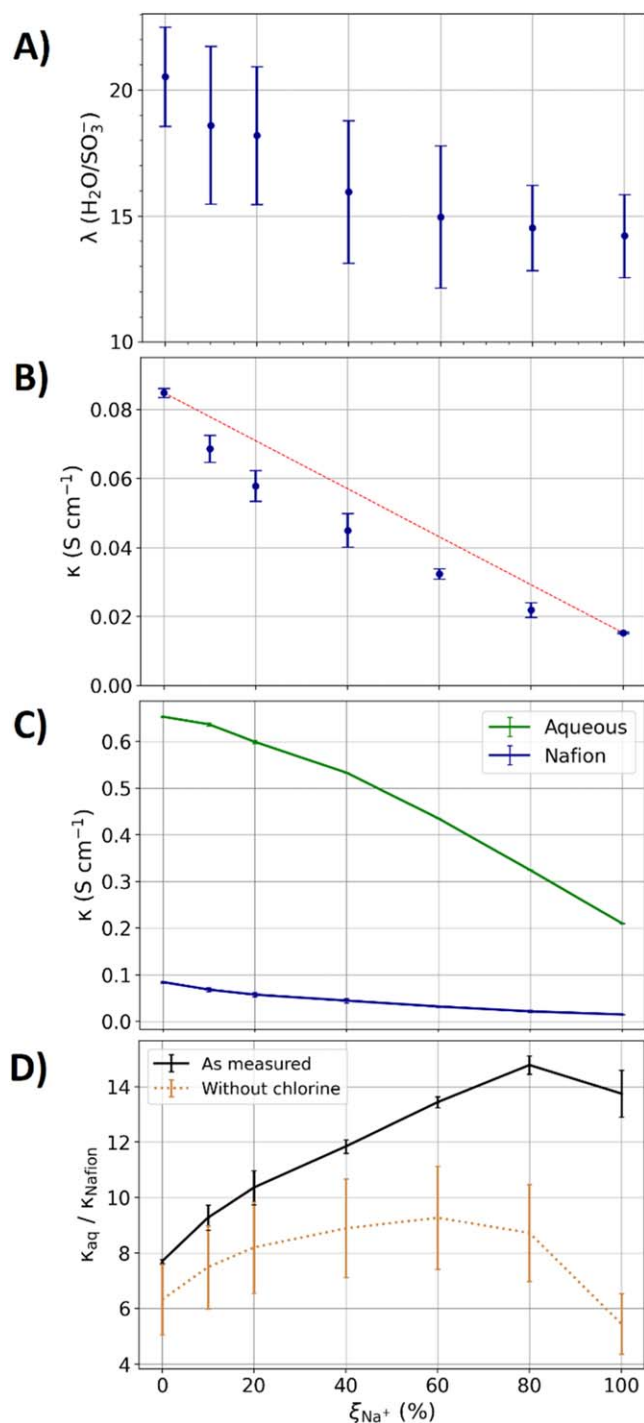


**Figure 2.** (A): Water uptake of Nafion after immersion in water as a function of the sodium ion content at 20 °C. (B): Conductivity of Nafion immersed in water as a function of the sodium ion content at 20 °C. The dotted red line represents a guide for the eye that linearly connects the conductivity of the H<sup>+</sup> form to that of the Na<sup>+</sup> form. (C): Data from (B) and conductivity of mixtures of aqueous solutions of HCl and NaCl with equal molarities as the protons and sodium-ions in the aqueous phase of Nafion. (D): Ratio of the conductivities shown in (C) and an estimation of the ratio that excludes the contributions of chloride ions to the conductivity of the aqueous solutions.

change due to the different framework of the aqueous solution and in the water channels of the Nafion membranes.

In a previous study,<sup>29</sup> the six-fold lower conductivity of protons in Nafion in comparison to that of aqueous solutions was related to

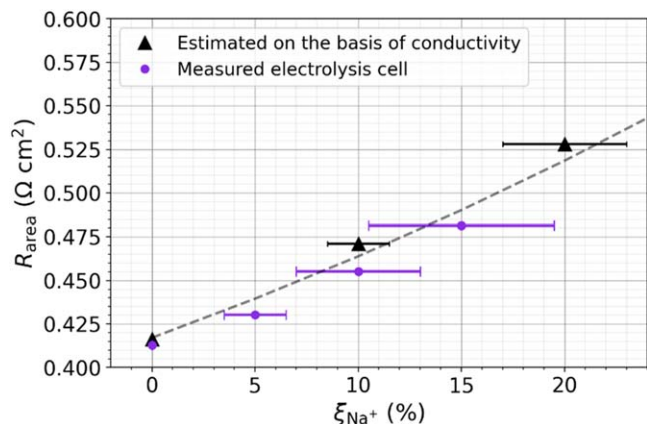


**Figure 3.** Area resistance of the cell at 20 °C as measured by the high frequency cell resistance (purple) and its estimation on the basis of the conductivity data from Fig. 2B (black). Dotted grey line: Guide to the eye.

microstructure of Nafion in terms of a reduced effective cross-section for the ion conduction and the tortuosity of the water channels. By adding sodium ions, the microstructure is changed due to the lower water uptake, which is expected to increase the tortuosity and reduce the effective cross-section for conduction. Figure 2D shows that the conductivity ratio of the cation conductivity increases until a sodium ion content of 60% is reached. Towards higher sodium ion contents the ratio decreases and comes back to a value of approximately six at a sodium ion content of 100%, albeit the geometric effects related to the reduced water uptake are expected to further increase the ratio. A similar cation conductivity ratio in the  $\text{H}^+$  and  $\text{Na}^+$  form despite the more pronounced geometric restrictions of the conductivity at the lower water uptake of the  $\text{Na}^+$  form may be explained by a reduced contribution of the Grothuss mechanism to the proton mobility in the water channels compared to that in aqueous solutions. Further investigations have to follow to understand the quite unexpected behavior of the cation conduction ratio as a function of the sodium ion content.

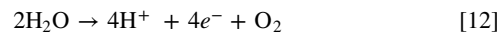
**Area resistance of the electrolysis cell.**—Figure 3 shows the area resistance of the electrolysis cell at 20 °C probed with alternating currents by impedance measurements for sodium ion contents of 0, 5, 10 and 15%. Moreover, Fig. 3 shows the area resistance of the electrolysis cell estimated on the basis of the measurements presented in Fig. 2. In detail, the membrane area resistance was calculated on the basis of Eq. 1 plus the area resistance of the cell assembly of  $0.16 \Omega \text{ cm}^2$ , that includes the resistances between the current collectors and the flow fields without the membrane. Measurements and estimations reasonably agree within the error approximations. The determined area resistance is with a sodium ion content of 15% approximately 14% higher than that without sodium ions. Thus, the conductivity changes by the sodium ion contents up to 15% are expected to just slightly impact the voltage current characteristics of the cell.

**Modeled current driven concentration gradients.**—The conductivity measurements presented above probe perturbations of the equilibrated membranes at alternating currents, where the membrane resistance is determined at frequencies above 100 Hz. Accordingly, ion movements on time scales smaller than 10 ms are examined. In contrast, direct current move the ions away from their equilibrium position and thus introduce a net ion movement on time scales that are orders of magnitudes larger. For more interested readers, a detailed comparison of the length scales of proton movements in Nafion under alternating current is discussed in the literature.<sup>29</sup> The aim of this section is to model the effect of direct currents on cation concentration gradients in PEMs during water electrolysis, which

facilitates the interpretation of experimental data at direct currents and the understanding of the physicochemical ion transport processes. Previous works examined the ion transport in aqueous solutions and the related concentration gradients in detail.<sup>28,30</sup> Here, we aim to adapt these models for the ion movement in Nafion as described in the “methods section” in detail. As discussed above, the model results for Nafion are semi-quantitative, as the model cannot fully represent the complex parameterization changes that result from a varying water content as a function of the sodium ion content and the related microscopic structure changes.

Figure 4 shows an example of the model outcome for a sodium ion content of 10% and a current density of  $1 \text{ A cm}^{-2}$  through the membrane. The  $x$ -axis shows the distance between the anode and the cathode multiplied by the tortuosity, representing the mean ion path with the detours through the three dimensional structure of the water channels in Nafion. The cations cannot move far away from the functional groups, as the electroneutrality and thus total charge must be maintained on a mesoscopic length scale. Within the framework of the model this means that in each of the 100 spatial increments between the anode and cathode the electroneutrality is balanced by the proton and sodium ions. Sodium ions and protons both can change positions, as both are freely mobile as dissociated ions in the aqueous phase. A parameter variation and the comparison to measurements are presented below.

Figure 4A shows the equilibrium state of the model framework with an equilibrated ion distribution. Figure 4B shows the simulation results after a current density of  $1 \text{ A cm}^{-2}$  was applied for 3 s. At the anode of the PEM cell protons enter the membrane as described by the anode reaction:



The sodium ions are transported to the cathode but cannot react there while protons are reduced at the cathode to hydrogen:



Hence, concentration gradients emerge, while the total amount of protons and sodium ions remains constant, as only their positions in the membrane are rearranged. The framework of electroneutrality thus captures the cations in the membrane, as they cannot diffuse into the pure water supply without a counter charge in the form of a mobile anion.

Figure 4C shows the modeled concentration gradients after 7.7 s at a current density of  $1 \text{ A cm}^{-2}$ . At the cathode, most protons are converted to hydrogen while sodium ions accumulate. Thus, the electrochemical proton reduction for the hydrogen evolution cannot be maintained as time proceeds further. To maintain the constant current in the model framework, water is reduced at the cathode:

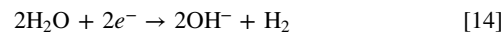
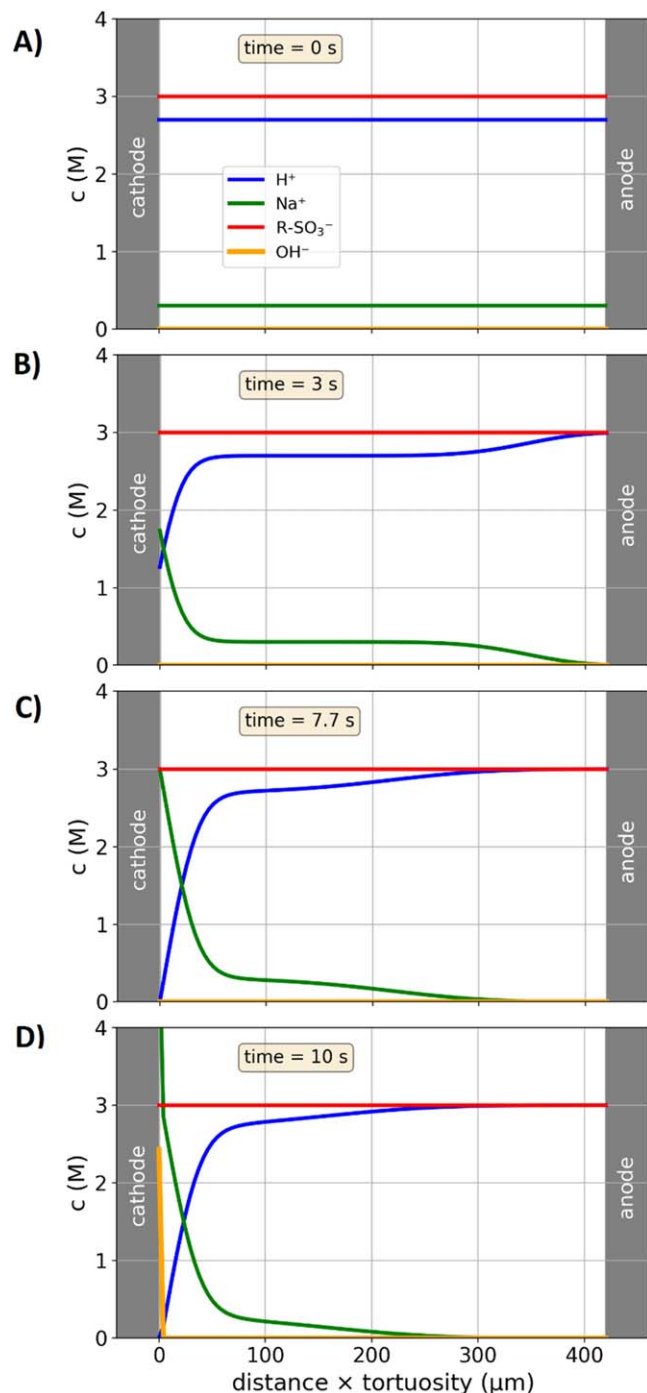
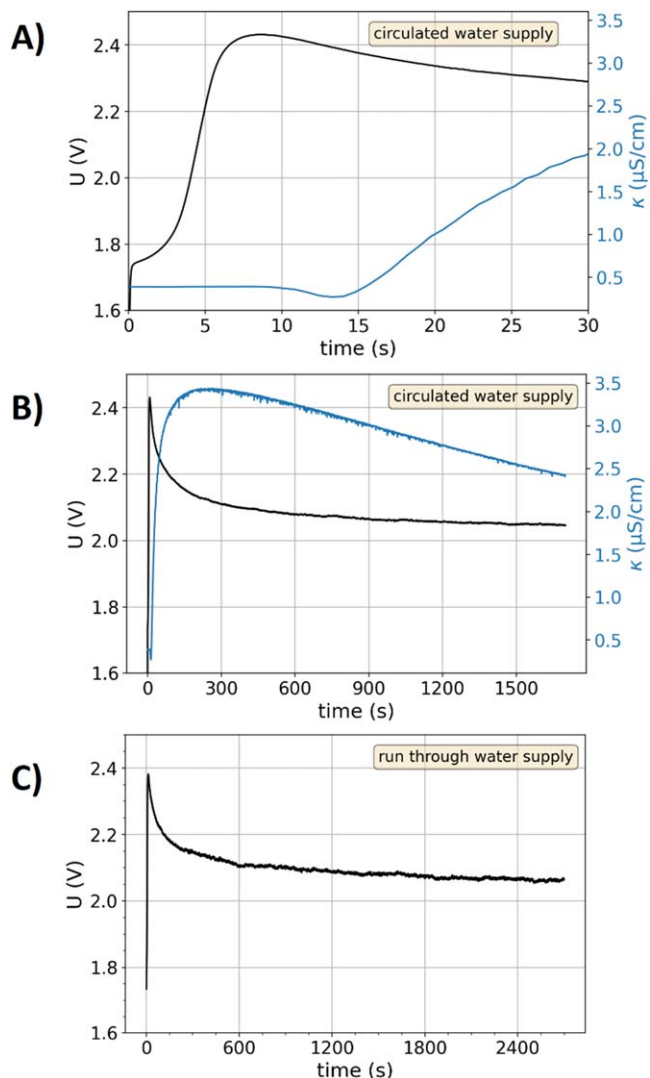


Figure 4D shows the concentration gradients after a modeled time of 10 s, showing that hydroxide ions occur at the cathode side of the membrane. As these hydroxide ions react with the intrinsic protons of the membrane, their penetration depth is expected to be rather small. Within the 100 compartments between the anode and cathode described by the model, the hydroxide ions do not reach the next neighbor compartment to the cathode. As hydroxide ions at least partly enter the membrane, the total amount of cations in the membrane is no longer restricted by the charge density of the functional groups. Thus, the concentration of cations in the compartment at the cathode increases which is in terms of the charge neutrality balanced by an increase of the concentration of hydroxide ions. In this case, sodium ions and hydroxide ions can diffuse pairwise from the cathodic catalyst layer to the cathodic water supply and thereby leave the membrane. This loss of sodium ions embodies a complex boundary condition that is not implemented in the model, as it depends on many parameters (see discussion below) and is considered in more detail by the following experiments. In the model,



**Figure 4.** Modeled concentration gradients of the ions inside the membrane during water electrolysis at a total current density of  $1 \text{ A cm}^{-2}$  with a sodium ion content of the membrane of 10%. The  $x$ -axis displays the product of the distance between the anode and cathode multiplied with the water channel tortuosity of 2.2. The current density in the aqueous phase is divided by an estimated volume fraction of the aqueous phase of 35%. (A) to (C): Concentration gradients forming over time. (D): The proton depletion at the cathode leads to the water reduction, so that hydroxide ions appear in the first spatial compartment at the cathode, while in the neighboring compartments hydroxide ions react with protons to water.

the cathode is implemented as a barrier to sodium ions, so that it is restricted to a constant amount of sodium ions in the membrane. Within this framework, the modeled gives a physical description of the ion transport as a function of time until hydroxide ions emerge, whereas afterwards the changes of the cathodic boundary conditions are not resolved.



**Figure 5.** Time-dependent cell voltages (left side, black) at  $80^\circ \text{C}$  and conductivity measurements of the supply water with a recirculated water supply (right side, blue), using a current density of  $1 \text{ A cm}^{-2}$  with a sodium ion content of the MEA of approximately 10%. (A) & (B): Operation with a recirculated water supply graphed on two different time scales. (C): After the measurements with the recirculated water circulation were conducted, the cell was rinsed with ultrapure water and the operation was continued with a run through supply of fresh ultrapure water.

**Electrolysis with poisoned membranes.**—Figure 5 shows the measured cell voltage of an electrolysis cell with sodium ion poisoning of 10% operated with a current density of  $1 \text{ A cm}^{-2}$ , aiming to discuss the following topics: (i) The time progression of the cell voltage and its relation to the physicochemical processes of the ion transport that were described by the above presented model. (ii) The influence of the operating condition of recirculated and run through water supply on the sodium ion loss of the membrane.

Figures 5A and 5B show the time-dependent behavior of the cell voltage of the MEA with a sodium ion content of 10% at a current density of  $1 \text{ A cm}^{-2}$  using a recirculated water supply for the anode and cathode, respectively. The cell voltage over time is characterized by three distinct points: (i)  $U_0$  at the beginning of the applied current, (ii)  $U_{\text{max}}$  which represents the peak cell voltage, and (iii)  $U_{10 \text{ min}}$  after the constant current density was applied for 10 min. The time-dependent cell voltage can be directly related to the modeled concentration gradients in Fig. 4. In the beginning, the sodium ions and protons are equally distributed within the membrane. With a sodium ion content of  $\xi_{\text{Na}^+} = 0.1$ , the overall cation concentration

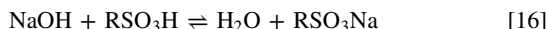
in the aqueous phase is 3 M with reference to a water uptake of  $\lambda = 18.5$  (see Fig. 2A). A proton concentration of 2.7 M results, which corresponds to a  $pH$  of  $-0.4$ . The potential of the hydrogen evolution reaction  $E_{HER}$  with reference to the potential of the standard hydrogen electrode (SHE) is  $pH$  dependent<sup>51</sup> as described by:

$$E_{HER} = -0.059 \text{ V} \times pH \quad [15]$$

Thus, the equilibrium potential of the hydrogen evolution is  $E_{HER} = 0.02 \text{ V}$  vs SHE in the beginning. As soon as the current is applied, the sodium ions accumulate at the cathode according to Fig. 4B while the amount of protons is reduced, resulting in a decrease of the acidity. Consequently,  $E_{HER}$  decreases, and therefore the cell voltage increases as the anodic potential remains mostly unaffected by the ion rearrangement in the membrane. Moreover, the overpotential for the HER on platinum is larger in the alkaline regime than in the acidic regime, which additionally decreases the cathodic potential.<sup>24</sup>

A steep increase of the cell voltage follows after applying the current for approximately 2 s, which is related to the ongoing reduction of the proton concentration at the cathode, which is displayed by the model in Figs. 4B and 4C. After operating the cell for approximately 8 s at  $1 \text{ A cm}^{-2}$ , the maximum voltage  $U_{max}$  is reached. The catalyst layer has a thickness of approximately  $10 \mu\text{m}$ , which exhibits different reaction zones with different  $pH$  values and varying amounts of sodium ions. As a result, the transition from an acidic to an alkaline regime at the cathode is a transient process that depends on the spatial dimensions of the cathode.

The cell voltage increases from  $U_0$  to  $U_{max}$  in Fig. 5A equals approximately 0.65 V. If this voltage difference is solely attributed to the change of  $E_{HER}$ , a cathodic alkalinity of  $pH = 10.6$  results. As soon as hydroxide ions are formed at the cathode, new dynamics come into play as they can pair with the sodium ions. The ion pairs can leave the membrane by mutual diffusion, neither disturbing the electroneutrality of the water supply nor that of the membrane. Moreover, the dissolved sodium hydroxide in the recirculated water supply can also react with the protons once again. The dissolved sodium hydroxide penetrating into the water supply increases the alkalinity of the cathodic water supply but decreases the alkalinity of the cathode in the MEA so that the cell voltage decreases after  $U_{max}$  was reached. The chemical reaction



describes the sodium balance of the water supply (left side) and the membrane (right side).

Figures 5A and 5B also show the conductivity of the cathodic water supply. After approximately 15 s of operation, the conductivity of the water supply starts to increase, whereas the maximum voltage  $U_{max}$  was already reached after 8 s. The water needs approximately 1 s from the cell output through the tubes to the cathodic water container. However, the time that the water needs to travel from the cathodic catalyst layer through the current collector and the flow field to the cathodic cell outlet is unknown. In addition, despite the water in the cathodic gas separator is stirred, it takes some time till the water entering the gas separator reaches the conductivity sensor. Thus, the exact moment that sodium hydroxide starts to get out of the membrane cannot be read out from the presented measurements. After approximately 200 s the conductivity of the cathodic supply water starts to slightly decrease. This decrease may be attributable to the absorption of  $\text{CO}_2$ , as sodium carbonate shows a lower conductivity than sodium hydroxide. Another explanation is the reabsorption of sodium ions by the membrane. The most drastic sodium ion removal took part in the first 150 s of the experiment. During this time, the concentration of sodium ions in the cathodic catalysts layer may be larger than afterwards, as it takes time from the sodium hydroxide solution at the cathodic catalysts layer to penetrate through the porous carbon current collector to the

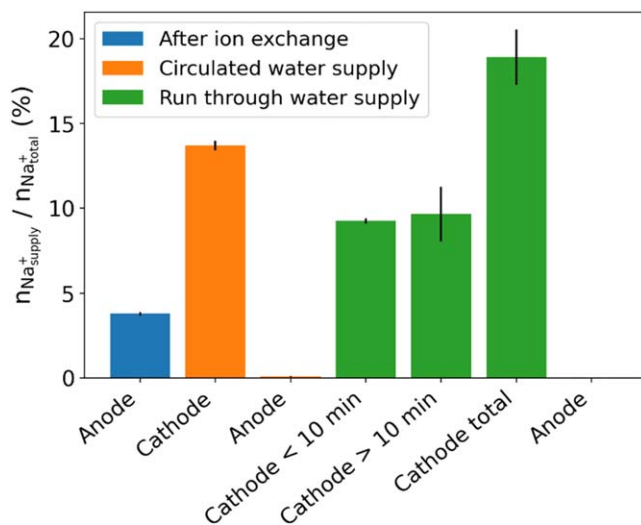


**Figure 6.** Sodium ion content in the water supply (normalized to the total amount of sodium ions of the ion exchange) after the ion exchange (blue), the operation with a recirculated water circle (orange) and run through water supply (green).

flow field. When the sodium hydroxide is partly transported away from the cathodic catalyst layer, the local sodium hydroxide concentration decreases, which thereby impacts the dynamic equilibrium described by Eq. 16. As a result, some of the previously washed out sodium hydroxide might be reabsorbed by the MEA. Moreover, the sodium concentration gradient in the membrane is expected to change over time as some of the sodium ions are leaving, which thus affects the balance between sodium ion washout and the reabsorption properties of the membrane.

Figure 5C shows the voltage progression over time of the same cell as that in Figs. 5A and 5B, but with a run through operation of the water supply. Again, the voltage increases after approximately 8 s to maximum of approximately 2.38 V. After 600 s the cell voltage decays to approximately 2.14 V. Afterwards, slow decrease of the cell voltage follows, ending at 2.08 V after a total time of 2700 s of this experiment. The once again cell voltage increase to  $U_{max}$  at the beginning underlines the previously postulated reabsorption of sodium ions and the dynamic behavior of the sodium ion washout that is described by Eq. 16. Until the protons are consumed at the cathode, the model gained a good understanding of the ion transport processes in the membrane. However, as soon as the cathode becomes alkaline, the ability of the pairs of sodium and hydroxide ions to leave the membrane complicate the physicochemical processes at the interphase between the membrane and the water supply. A fraction of the hydroxide ions produced at the cathode may be directly transported in the electric field of the MEA towards the inside of the membranes, where they instantaneously react with the protons. Thus, as the ion movement is expected to influence the transfer rate of sodium and hydroxide ion pairs towards the water supply, the diffusion of the ions along the concentration gradient between the water supply and the catalyst layer may be damped. These microscopic effects in the cathodic catalyst layer exceeds the capabilities of the presented model and require a more advanced understanding of the interfaces between the water supply, catalyst layer and membrane.

Figure 6 shows the sodium ion content of the supply water at the end of the ion exchange procedure, the recirculated operation of the water supply (Figs. 5A and 5B) and the run through operation of the water supply (Fig. 5C). After purging the sodium hydroxide solution along the anode of the cell to replace 10% of the membrane's protons with sodium ions, approximately 4% of the entire sodium hydroxide used remained in the water supply, which means that most of the sodium ions were absorbed by the membrane. The remaining

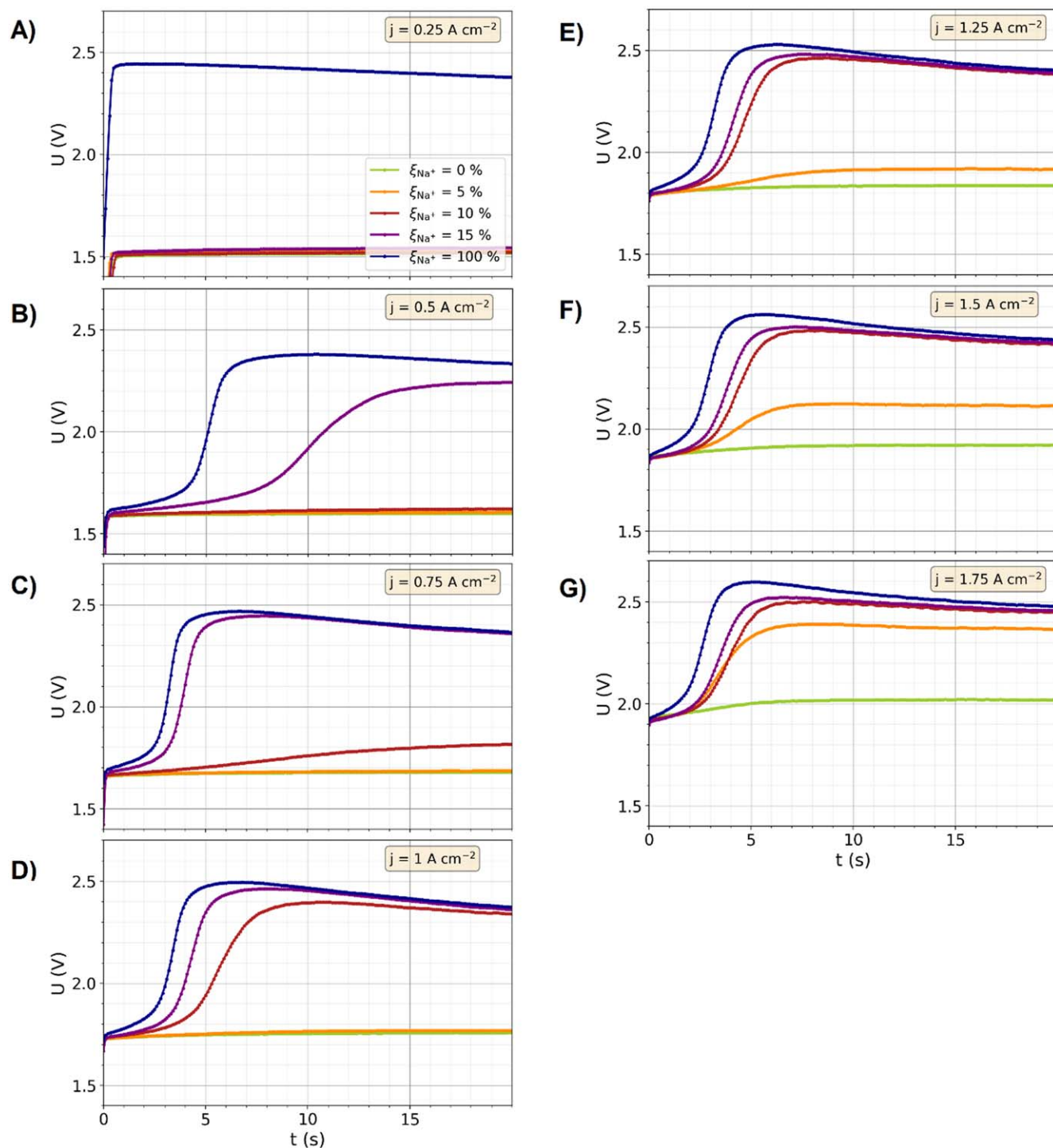


**Figure 7.** Time progression of the cell voltage for a variation of the sodium ion content of 0, 5, 10, 15 and 100% as characterized by the current density profile that is shown in Fig. 1.

sodium ion content of water supply was washed out by rinsing with ultrapure water. After the experiment shown in Fig. 5B was finished, approximately 14% of the initially absorbed sodium ions were found in the cathodic water circulation, which were washed out by the electrochemical current. The anode did not contain a resolvable amount of sodium ions. After the experiment with the run through water supply (Fig. 5C), approximately 9% off the initially absorbed sodium ions were washed out after 10 min of operation. Another approximately 10% were rinsed out during the further 35 min that the experiment was conducted. After all the experiments in Fig. 5,

the MEA lost approximately 33% of the initially introduced sodium ions.

**Variation of current density and sodium ion content.**—In the following, the effect of current density and sodium ion content on the cell voltage is characterized by applying the current density profile shown in Fig. 1 to the electrolysis cell with sodium ion contents of the membrane of  $\xi_{\text{Na}^+}$  of 0, 0.05, 0.1, 0.15 and 1. Figure 7 shows the time resolved results of these measurements. At a current density of  $1 \text{ A cm}^{-2}$ , the MEA with a sodium ion content of 5%

**Table II.** Experimental times to reach a cell voltage increase of 0.1 V and 0.6 V in comparison to the modeled times to reach a proton depletion at the cathode for selected measurements displayed in Fig. 7.

$\xi_{\text{Na}^+}$ (%)	$j$ (A cm <sup>-2</sup> )	$t_{\text{exp}}$ @ $\Delta U = 0.1$ V	$t_{\text{exp}}$ @ $\Delta U = 0.6$ V	$t_{\text{sim}}$
5	1.25	—	—	—
5	1.5	4	—	9.4
5	1.75	2.5	—	6.8
10	0.5	—	—	—
10	0.75	12	—	13.0
10	1	4.5	8	7.7
15	0.25	—	—	—
15	0.5	7	14	15.7

yields a constant voltage profile over time, as the concentration gradients in the membrane do not lead to a proton depletion at the cathode. The MEAs prepared with higher sodium ion contents show a distinct voltage increase from  $U_0$  to  $U_{\text{max}}$  in the examined current density window. The time for this voltage increase decreases with higher a sodium ion content, as more sodium ions lead to a faster proton depletion at the cathode.

Table II summarizes the times to reach a cell voltage increase  $\Delta U$  of 0.1 V and 0.6 V of the experimental data in Fig. 7 and the modeled times to reach a proton depletion at the cathode. A voltage increase of  $\Delta U = 0.1$  V means a significant impact on the cell characteristics by changes of the cathodic reaction in a less acidic environment. With a voltage increase of  $\Delta U$  of 0.6 V or higher, the cathode is definitely alkaline and the MEA loses sodium ions. Thus, when applying the current density profile of Fig. 1, all data that comes after a voltage increase  $\Delta U$  of 0.6 V is not relatable to the initially adjusted sodium ion content. Thus, only the experiments with a defined sodium ion content of the membrane are compared to the modeled results in Table II. The main error for the experimental data comes from the sodium ion content, as it is unclear how much penetrates to the membrane material below the sealing (see “methods section”), whereas small differences in the sodium ion content have a drastic effect on the times of the modeled proton depletion.

At a sodium ion content of 5% and a current up to 1.25 A cm<sup>-2</sup>,  $U_{\text{max}}$  and  $U_0$  are almost equal, which means that proton depletion does not play a significant role. The diffusion of sodium ions and protons in the membrane partly equilibrate the concentration gradients and thus protons are provided at the cathode. Similarly, the model does not predict a proton depletion at the cathode. Increasing the current density to 1.5 A cm<sup>-2</sup> leads to a significant difference of  $U_{\text{max}}$  in comparison to  $U_0$ . After approximately 4 s, the cell voltage is increased by 0.1 V, while the cell voltage increase  $\Delta U$  is smaller than 0.25 V during the entire experiment. Thus, the cathodic environment remains acidic, whereas a proton shortage in parts of the cathodic catalyst layer leads to low amounts of hydroxide ions. The model predicts a proton depletion after approximately 9 s, which is higher than the observed time to reach the maximum voltage increase. The experimental data suggest that a proton shortage at the cathode appears, but this is not enough to turn the electrode completely alkaline. At a current density of 1.75 A cm<sup>-2</sup>,  $U_{\text{max}}$  is reached after approximately 7 s with a voltage increase  $\Delta U$  of approximately 0.5 V. The model here also predicts a proton depletion after approximately 7 s, for which the experimental and model data show a good match.

At a sodium content of 10% and a current density of 0.5 A cm<sup>-2</sup>, experiment and model do not show a proton depletion at the cathode. At 0.75 A cm<sup>-2</sup> the cell voltage increases after 12 s by approximately 0.1 V, which is similar to the modeled time of 13 s for a proton depletion at the cathode. At 1 A cm<sup>-2</sup>, the model predict 7.7 s for a proton depletion at the cathode whereas the measurements indicate a voltage increase of 0.6 V after 8 s. In the case of a sodium ion content of 15% and a current density of 0.25 A cm<sup>-2</sup>, experiment

and model do not show a proton depletion at the cathode. At 0.5 A cm<sup>-2</sup>, the observed voltage increase of 0.6 V takes place after 14 s, roughly matching to the modeled time of 15.7 s for a proton depletion. Accordingly, despite the model with its simplifications (see “methods section”) can be only seen as a semi-quantitative approach to describe the ion transport in the electrolysis cell, the predicted times for the cathodic proton depletion roughly agree with the measured data. To summarize, in the cases of distinct voltage increases by 0.6 V, the experimentally overserved times for this voltage increase and the modeled time for the proton depletion match. In the cases of smaller voltage increases, it remains unclear, how much the proton depletion affects the sensible tipping point at the cathodic transition from a mainly acidic to a mainly alkaline state.

Figure 8A to 8C show the three characteristic voltages  $U_0$ ,  $U_{\text{max}}$ , and  $U_{\text{end}}$  (defined in Figs. 5A and 5B) that were extracted from the measurements graphed in Fig. 7. The voltages  $U_0$  are almost equal for all different sodium ion contents except for the measurement with 100% sodium content at the first step of the current density profile. In this case, the cathodic environment instantaneously turns into an alkaline regime, as protons are not available at the cathode so that the hydrogen formation directly starts via the alkaline pathway by the water reduction. In this case, after the first step of the current profile,  $U_0$  is similar to those of the other sodium ion contents. Thus, at the first step of the current density profile a significant amount of sodium ions of the membrane is washed out to the water supply, which is in the 10 min break between the current steps not completely reabsorbed. The conductivity decrease of the membrane by sodium ion uptake up to contents of 15% are expected to have just a small impact on the conductivity of the Nafion membranes (shown in Fig. 3), as reflected by almost equal starting voltages  $U_0$ . The higher the sodium ion content, the lower is the current density that leads to a deviation of  $U_{\text{max}}$  relative to the H<sup>+</sup> form.

If the voltage increase  $\Delta U$  between  $U_0$  and  $U_{\text{max}}$  is larger than 0.5 V, the voltage  $U_{10 \text{ min}}$  is significantly smaller than  $U_{\text{max}}$ . This decrease of the cell voltage indicates that sodium ions are partly washed out. However, all cases with a significantly higher  $U_{\text{max}}$  compared to the H<sup>+</sup> form also lead to a higher  $U_{10 \text{ min}}$  relative to the H<sup>+</sup> form, which means that the electrochemical sodium ion removal does not bring the membrane back to its pristine state. Figure 8D shows the voltage-current characteristics of the membrane in the pristine H<sup>+</sup> form directly after the cell assembly. Moreover, the voltage-current characteristic of the MEA in the restored H<sup>+</sup> form is graphed, for which the MEA was transferred to the Na<sup>+</sup> form followed by rinsing in sulfuric acid and subsequently run through rinsing with ultrapure water. Similarly to the conductivity measurements discussed above, rinsing with sulfuric acid fully reversibly transfers the Na<sup>+</sup> to the H<sup>+</sup> form. Hence, the sodium ion poisoning itself is reversible, as diffusion leads in case of an oversupply of protons in the water supply to an exchange of the sodium ions. However, the equilibrium described by Eq. 16 hinders the ion transport driven wash out of sodium ions to completely remove all sodium ions from the membrane.

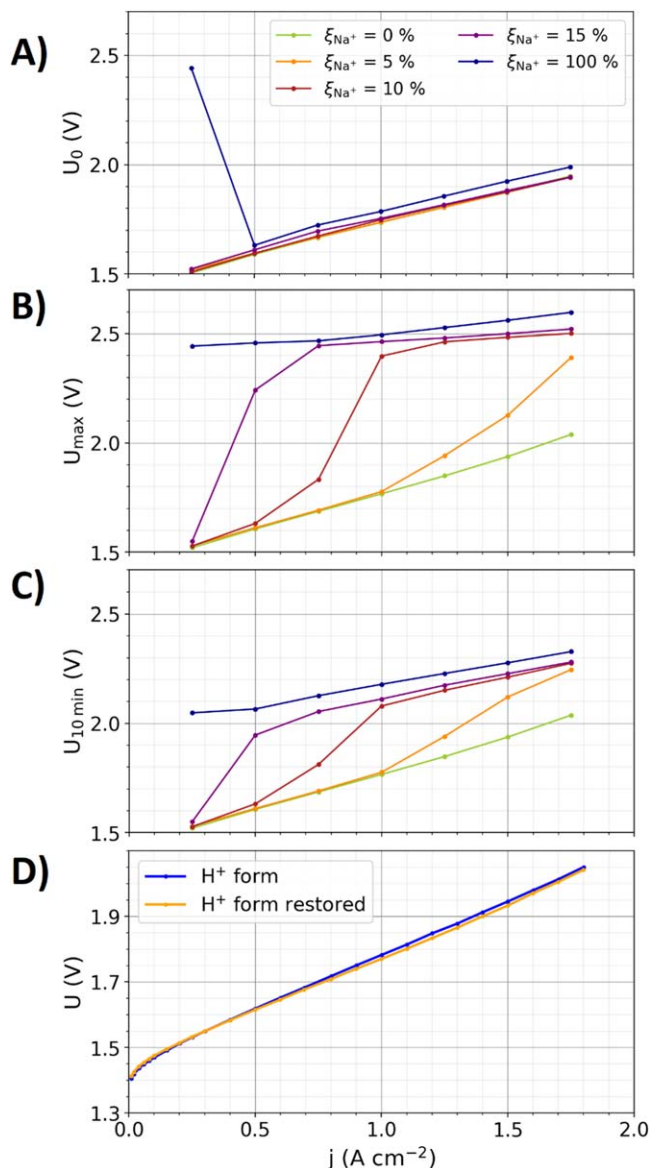


**Figure 8.** (A) to (C): The three characteristic voltages  $U_0$ ,  $U_{\max}$ , and  $U_{10,\min}$  extracted from the measurements graphed in Fig. 7 as a function of the current density. (D): Voltage current characteristic at 80 °C in the pristine form (without any sodium ion contamination) and a restored proton state, in which the introduced sodium ion content of 10% was treated by rinsing with sulfuric acid and subsequent removing of the acidic residuals.

**Remarks towards application of PEM water electrolysis.**—The sodium ion accumulation in the membrane seems unavoidable during the operation of electrolyzers in industrial application conditions, as sodium chloride is typically dominating salt impurities in pure water supply while water purification techniques reduce the salt content but cannot avoid these unless very sophisticated and expensive purification systems are employed.<sup>52,53</sup> Previous works<sup>20,23</sup> and data in the supporting information show the effect of sodium chloride in the anodic water supply on the cell voltage. As the supplied water is electrolyzed, the sodium ions are expected to accumulate in the MEA while the chloride ions will be oxidized to chlorine and thus are expected to leave via the gas phase. Thus, it is only a matter of time until sodium ion-poisoning results in a cell voltage increase. Figure 9 shows the estimated sodium ion accumulation in a Nafion N117 membrane over time assuming a sodium ion content in the water supply of 1  $\mu\text{M}$  NaCl. This estimated sodium ion content in the membrane is calculated by the ratio of the sodium ion content in the water supply times the ratio of the amount of

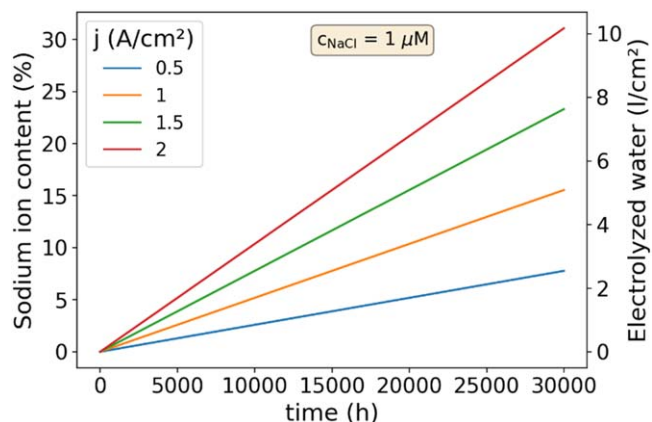


**Figure 9.** Modeled sodium ion accumulation in a N117 membrane (left) and amount of electrolyzed water per square centimeter of cell area (right) as a function time for four different current densities. The calculations are based on a concentration of 1  $\mu\text{M}$  of NaCl in the anodic supply water and the assumption that all sodium ions of the water supply are trapped inside the membrane.

electrolyzed water  $n_{\text{H}_2\text{O}}$  to the amount of functional groups  $n_{\text{Nafion}}$  of the Nafion membrane

$$\xi_{\text{Na}^+} = \frac{c_{\text{NaCl}}}{c_{\text{NaCl}} + c_{\text{H}_2\text{O}}} \frac{n_{\text{H}_2\text{O}}}{n_{\text{Nafion}}} \quad [17]$$

where  $c_{\text{NaCl}}$  denotes the concentration of sodium ions,  $c_{\text{H}_2\text{O}} = 55 \text{ M}$  the concentration of water,  $n_{\text{H}_2\text{O}}$  the amount of electrolyzed water per cm<sup>2</sup> of the electrolysis cell and  $n_{\text{Nafion}}$  the amount of functional groups of the Nafion membrane per cm<sup>2</sup>. Using Faradays law, the amount of electrolyzed water was calculated to:  $n_{\text{H}_2\text{O}} = \frac{ij}{4F}$ . Using a membrane area weight of 360 g m<sup>-2</sup> in the dry state,  $n_{\text{Nafion}}$  was calculated as the ratio of the membrane area weight to equivalent weight. By comparison of Figs. 9 with 8, one can estimate the current density at which the sodium ion poisoning of a Nafion N117 membrane will lead to a significant impact on the cell voltage. For example, Fig. 8 showed that at a current density of 1.5 A cm<sup>-2</sup> a sodium ion content of 5% will lead to a significant impact on the cell voltage, which is reached with 1  $\mu\text{M}$  of NaCl in the supply water reached after approximately 6000 h of operation.

The model for the ion transport in PEMs presented in this work is capable to semi-quantitatively estimate the effect of multidimensional parameter space of sodium ion content, membrane thickness and current density on the sodium ion depletion at the cathode, in which conductivities and diffusion coefficients serve as input parameters. Hence, this model can be helpful to estimate of the effect of sodium ion poisoning on the cell properties at various membranes thicknesses or temperatures. Moreover, with the data presented in Fig. 8, the sodium ion content of a Nafion N117 can be estimated on the basis of voltage-current characteristics at a cell temperature of 80 °C. The measurements showed a complex dynamic of the sodium ion wash out and its reabsorption, which may also help to partly cure the poisoning by for example applying high current densities in combination with the run through operation of the water supply, which allows to at least partly electrochemically wash out sodium ions from the membrane. Moreover, the understanding of the ion transport and the interfacial effects might help to improve the ion removal technique with CO<sub>2</sub> purging that is reported by Babic et al.,<sup>24</sup> whereas the influence of CO<sub>2</sub> on the equilibrium described by Eq. 16 displays an interesting topic for future works. In the case of the operation of the electrolysis cell without a cathodic water supply, less liquid water at the cathode might reduce the rate for the sodium ion removal, which is another topic that also has to be addressed in future works.

## Conclusions

In this study, the ion transport through a sodium-ion poisoned Nafion membrane is examined under alternating currents and direct currents. The conductivities of Nafion membranes and aqueous acidic solutions with varying sodium ion contents were measured by impedance spectroscopy. Differences in the conductivities of both electrolytes were discussed and related to the microstructural change in the membrane that result from the impact of sodium ions on the water uptake. These conductivities are related to the area resistances of an electrolysis cell with different sodium ion contents. A physical model to describe the ion transport in a sodium ion poisoned Nafion membrane was introduced, which describes concentration gradients of sodium ions and protons under direct current operation. The dynamics of the cell voltage of an electrolyzer with a Nafion-based membrane electrode assembly (MEA) with sodium ion poisoning were examined while the sodium ion removal from the membrane was monitored by conductivity measurements of the water supply and ICP-OES analysis. The cell voltages as a function of time were related to the modeled result for the ion transport, which revealed their relation to the time scales for the rearrangement of ions in the membrane. The parameters space in which a cathodic sodium ion accumulation leads to an accompanied proton depletion is analyzed, showing that a drastic increase of the cell voltage by an alkalized cathode can be reached with just small amounts of sodium ion poisoning. Hydroxide ions from water reduction and dissociated sodium ions can leave the membrane pairwise via mutual diffusion into the water supply without disturbing the electroneutrality of ions in the membrane and the water supply. With regard to application, the time to observe the effect of sodium ion accumulation in the membrane on the cell voltage is estimated.

## Acknowledgments

This work was supported by the German Federal Ministry of Education and Research (BMBF) through the project DERIEL (03HY122C).

## Supporting information

The supporting information to this article contains:

- Schematic sketches of the used electrochemical cells
- Impedance spectra of a Nafion specimen
- Data on the reversibility of the conductivity of Nafion
- Comparison of the sodium ion content prepared by electrolysis of sodium chloride and rinsing with sodium hydroxide
- Detailed discussion of the model parameterization
- The source code (Python) for the model

## ORCID

Maximilian Schalenbach  <https://orcid.org/0000-0002-2040-2483>

## References

1. J. O. M. Bockris, *Science* (80), **176**, 1323 (1972).
2. L. Barreto, A. Makihira, and K. Riahi, *Int. J. Hydrogen Energy*, **28**, 267 (2003).
3. M. Schalenbach, G. Tjarks, M. Carmo, W. Lueke, M. Mueller, and D. Stolten, *J. Electrochem. Soc.*, **163**, F3197 (2016).
4. S. J. Peighambaroust, S. Rowshanzamir, and M. Amjadi, *Int. J. Hydrogen Energy*, **35**, 9349 (2010).
5. D. W. Shin, M. D. Guiver, and Y. M. Lee, *Chem. Rev.*, **117**, 4759 (2017).
6. K. A. Mauritz and R. B. Moore, *Chem. Rev.*, **104**, 4535 (2004).
7. F. I. Allen, L. R. Comolli, A. Kusoglu, M. A. Modestino, A. M. Minor, and A. Z. Weber, *ACS Macro Lett.*, **4**, 1 (2015).
8. K. D. Kreuer, *J. Memb. Sci.*, **185**, 29 (2001).
9. S. Slade, S. A. Campbell, T. R. Ralph, and F. C. Walsh, *J. Electrochem. Soc.*, **149**, A1556 (2002).
10. S. Shiva Kumar and V. Himabindu, *Mater. Sci. Energy Technol.*, **2**, 442 (2019).
11. M. Carmo, D. L. Fritz, J. Mergel, and D. Stolten, *Int. J. Hydrogen Energy*, **38**, 4901 (2013).
12. Q. Feng, X. Yuan, G. Liu, B. Wei, Z. Zhang, H. Li, and H. Wang, *J. Power Sources*, **366**, 33 (2017).
13. S. A. Grigoriev, K. A. Dzhuz, D. G. Bessarabov, and P. Millet, *Int. J. Hydrogen Energy*, **39**, 20440 (2014).
14. M. Schalenbach, A. R. Zeradjanin, O. Kasian, S. Cherevko, and K. J. J. Mayrhofer, *Int. J. Electrochem. Sci.*, **13**, 1173 (2018).
15. W. Xu and K. Scott, *Int. J. Hydrogen Energy*, **35**, 12029 (2010).
16. S. A. Grigoriev and A. A. Kalinnikov, *Int. J. Hydrogen Energy*, **42**, 1590 (2017).
17. M. Mandal, M. Moore, and M. Secanell, *ACS Appl. Mater. Interfaces*, **12**, 49549 (2020).
18. M. Carmo, D. L. Fritz, J. Mergel, and D. Stolten, *Int. J. Hydrogen Energy*, **8**, 4901 (2013).
19. M. Chandresris, V. Médeau, N. Guillet, S. Chelghoum, D. Thoby, and F. Fouda-Onana, *Int. J. Hydrogen Energy*, **1** (2014).
20. L. Zhang, X. Jie, Z. G. Shao, Z. M. Zhou, G. Xiao, and B. Yi, *Int. J. Hydrogen Energy*, **37**, 1321 (2012).
21. A. S. Aricò, S. Siracusano, N. Brigioglio, V. Baglio, A. Di Blasi, and V. Antonucci, *J. Appl. Electrochem.*, **43**, 107 (2013).
22. C. Xiang, K. M. Papadantonakis, and N. S. Lewis, *Mater. Horizons*, **3**, 169 (2016).
23. L. Zhang, X. Jie, Z. G. Shao, X. Wang, and B. Yi, *J. Power Sources*, **241**, 341 (2013).
24. U. Babic, M. Zlobinski, T. J. Schmidt, P. Boillat, and L. Gubler, *J. Electrochem. Soc.*, **166**, F610 (2019).
25. A. K. Sethurajan, S. A. Krachkovskiy, I. C. Halalay, G. R. Goward, and B. Protas, *J. Phys. Chem. B*, **119**, 12238 (2015).
26. M. Klett, M. Giesecke, A. Nyman, F. Hallberg, R. W. Lindström, G. Lindbergh, and I. Furó, *J. Am. Chem. Soc.*, **134**, 14654 (2012).
27. S. A. Krachkovskiy, A. D. Pauric, I. C. Halalay, and G. R. Goward, *J. Phys. Chem. Lett.*, **4**, 3940 (2013).
28. M. Schalenbach, B. Hecker, B. Schmid, Y. E. Durmus, H. Tempel, H. Kungl, and R. Eichel, *Electrochem. Sci. Adv.*, e2100189 (2022).
29. M. Schalenbach, W. Lueke, W. Lehnert, and D. Stolten, *Electrochim. Acta*, **214**, 362 (2016).
30. M. Schalenbach, Y. E. Durmus, H. Tempel, H. Kungl, and R.-A. Eichel, *Sci. Rep.*, **12**, 1 (2022).
31. M. Zlobinski, U. Babic, M. Fikry, L. Gubler, T. J. Schmidt, and P. Boillat, *J. Electrochem. Soc.*, **167**, 144509 (2020).
32. Y. Sone, P. Ekdinge, and D. Simonsson, *J. Electrochem. Soc.*, **143**, 1254 (1996).
33. P. Vanysek, *CRC Handbook of Chemistry and Physics* (CRC Press, Boca Raton, FL) p. 1 (2015).
34. G. M. Kontogeorgis, B. Maribo-Mogensen, and K. Thomsen, *Fluid Phase Equilib.*, **462**, 130 (2018).
35. Q. Zhao, P. Majsztrik, and J. Benziger, *J. Phys. Chem. B*, **115**, 2717 (2011).
36. M. Schalenbach, M. Hoeh, J. Gostick, W. Lueke, and D. Stolten, *Phys. Chem. C*, **119**, 25156 (2015).
37. J. R. Varcoe et al., *Energy Environ. Sci.*, **7**, 3135 (2014).
38. N. Agmon, *Chem. Phys. Lett.*, **244**, 456 (1995).
39. D. Marx, *ChemPhysChem*, **7**, 1848 (2006).
40. I. A. Stenina, P. Sistat, A. I. Rebrov, G. Pourcelly, and A. B. Yaroslavtsev, *Desalination*, **170**, 49 (2004).
41. K. D. Kreuer and G. Portale, *Mater. Views*, **23**, 5390 (2013).
42. C. E. Evans, R. D. Noble, S. Nazeri-Thompson, B. Nazeri, and C. A. Koval, *J. Memb. Sci.*, **279**, 521 (2006).
43. J. T. Gostick and A. Z. Weber, *Electrochim. Acta*, **179**, 137 (2015).
44. A. Z. Weber and J. Newman, *J. Electrochem. Soc.*, **151**, A311 (2004).
45. K. M. Vetter, J. Härtl, D. Reinisch, T. Reichbauer, N. Martić, K. O. Hinrichsen, and G. Schmid, *ChemElectroChem*, **9**, e202101165 (2022).
46. J. C. Bendert, D. D. Papadias, and D. J. Myers, *J. Electrochem. Soc.*, **157**, B1486 (2010).
47. N. H. Jalani and R. Datta, *J. Memb. Sci.*, **264**, 167 (2005).
48. M. H. Eikerling and P. Berg, *Soft Matter*, **7**, 5976 (2011).
49. T. Okada, Y. Ayato, M. Yuasa, and I. Sekine, *J. Phys. Chem. B*, **103**, 3315 (1999).
50. J. G. Goodwin, K. Hongsirikarn, S. Greenway, and S. Creager, *J. Power Sources*, **195**, 7213 (2010).
51. M. Pourbaix, *Atlas of Electrochemical Equilibria in Aqueous Solutions* (NACE International, Cebelcor, Houston) 2nd ed., p. 644 (1974).
52. G. Folaranmi, M. Bechelany, P. Sistat, M. Cretin, and F. Zaviscka, *MDPI Membranes*, **10**, 96 (2020).
53. M. Metzger, M. M. Besli, S. Kuppam, S. Hellstrom, S. Kim, E. Sebt, C. V. Subban, and J. Christensen, *Energy Environ. Sci.*, **13**, 1544 (2020).